Investigating ground-state properties of neutron-rich nuclei with $Z = 98$ - 104 in the reflection-asymmetric relativistic mean-field theory*

Yu-Ting Qiu (仇玉亭) Jian-You Guo (郭建友)†

School of Physics, Anhui University, Hefei 230601, China

Abstract: A systematic microscopic analysis of the ground-state properties for the neutron-rich even-even nuclei with $Z = 98 - 104$ and $N = 170 - 210$ is performed using the reflection-asymmetric relativistic mean-field theory with the NL3, NL3*, and PK1 effective interactions. The pairing effect is taken into account via the BCS approximation with a constant pairing gap. It is found that the octupole deformation significantly influences the physical properties of Cf, Fm, No, and Rf isotopes. Particularly, incorporating the reflection-asymmetric degree of freedom enhances the binding energies, quadrupole deformations, and neutron, proton, and charge radii for nuclei near $N = 184$ and $N = 196$. The possible candidates, $N \approx 184$ and $N \approx 196$, for the new neutron octupole magic number are predicted in the present calculations. The effect of the size of the pairing correlations on the octupole deformation of nuclei is examined by varying the pairing gap. It is found that the octupole deformation decreases as the pairing gap increases. This reduction underscores the critical role of precise treatment of the pairing correlations in achieving a reliable prediction of the octupole deformation of nuclei. Additionally, we further investigate the sensitivity of the nuclear properties to the Coulomb interaction. The results show that the inclusion of the Coulomb interaction increases quadrupole and octupole deformations as well as neutron, proton, and charge radii but leads to a marked reduction in binding energies. These conclusions remain consistent across the calculations employing the NL3, NL3*, and PK1 parameter sets. To more broadly validate the robustness of the present findings, further investigation based on other types of effective interactions and pairing forces is worthwhile.

Keywords: Relativistic mean-fiield theory, Ground-state property, Octupole deformation, Coulomb interaction

DOI: 10.1088/1674-1137/ae6a83 **CSTR:**

I. INTRODUCTION

The shape or deformation of the atomic nucleus, as one of its most fundamental properties, plays a pivotal role in elucidating various exotic nuclear phenomena, e.g., shape coexistence [1], chiral rotation [2], wobbling motion [3], and fission [4]. The occurrence of spontaneous symmetry breaking results in nuclear shapes with various spatial symmetries. Throughout the nuclear chart, the ground states of most nuclei are well-known to have axial reflection-symmetric shapes, which are often described by the quadrupole deformation β_{20}. However, around some specific proton and/or neutron numbers, i.e., the so-called octupole magic numbers 34, 56, 88, and 134 [5, 6], the nuclei spontaneously break spatial reflection symmetry, favoring the axial reflection-asymmetric ground-state shape characterized by octupole deformation β_{30} [7]. In a mean-field description of the nucleus, the emergence of octupole deformation can be ascribed to the coupling between intruder (N, l, j) and normal-parity $(N-1, l-3, j-3)$ single-particle orbitals near the Fermi surface [8−10].

The octupole degree of freedom significantly influences not only the properties of nuclear ground and excited states [11−20] but also holds the key to a microscopic understanding of the fission process [21−28], cluster radioactivity [29], and stability of superheavy elements [30, 31]. Therefore, the study of octupole deformation in nuclei has remained an active research field in both theoretical and experimental nuclear physics for the past few decades. To date, advances in radioactive-ion beam facilities have enabled nuclear physicists to identify experimental evidence for permanent octupole deformation in neutron-rich lanthanides near ^{144}Ba

Received 26 January 2026; Accepted 6 May 2026

* This work was partly supported by the National Natural Science Foundation of China under Grants No. 12475115, No. 11935001, and No. 11575002, the Anhui project (Z010118169), the Heavy Ion Research Facility in Lanzhou (HIRFL) (HIR2021PY007), and the Graduate Research Foundation of the Education Ministry of Anhui Province under Grant No. YJS20210096

† E-mail: jianyou@ahu.edu.cn

($N=88, Z=56$) [32, 33] and light actinides near ^{222}Ra ($N=134, Z=88$) [34, 35]. Furthermore, fingerprints of octupole correlations have also been found in ^{224,226}Rn [36], ^{228}Ra [35], and ^{228}Th [37]. These findings strongly support the proposed octupole magic numbers 56, 88, and 134. In parallel, to support the evidence of octupole deformation and further understand the novelties associated with octupole correlations, physicists have developed or employed a variety of theoretical models to explore the ground-state properties and structures of octupole-deformed nuclei, such as the macroscopic-microscopic (MM) model [5, 38, 39], the reflection-asymmetric shell model [40, 41], the quadrupole-octupole collective Hamiltonian [42−44], the interaction boson model [45−49], the generator coordinate method [50−54], and the microscopic calculations based on nonrelativistic energy density functionals (EDFs) [55−60].

The covariant density functional theory (CDFT) [61−65], as one of the most powerful theories in nuclear physics, has been successfully applied to describe the ground-state properties across the nuclear landscape, from light nuclei to superheavy systems. Therefore, it is also appropriate to study the ground-state octupole deformations of atomic nuclei by utilizing the CDFT with the reflection-asymmetric degree of freedom. The first analysis of octupole shapes of nuclei within the CDFT framework has been conducted in Ref. [66]. This study has explored the potential for stable octupole deformation in the ground states of Ra isotopes and the influence of octupole deformation on the static fission properties of actinides. Starting from the pioneering work of Ref. [66], the CDFT has been widely used in the investigation of reflection-asymmetric nuclear shapes [67−71] and has provided a reasonable description of the octupole shape phase transition and shape coexistence phenomena [12, 72−75]. Particularly, to more appropriately describe axially symmetric octupole-deformed nuclei, the reflection-asymmetric relativistic mean-field (RASRMF) theory in the two-center harmonic oscillator (TCHO) basis has been developed by Geng *et al*. [76]. Based on the RASRMF theory, the octupole deformations in the nuclear ^{226}Ra [76], as well as La [77], Sm [78], Ba [79], Th [80], Ce [81], and Dy [82] isotopes, have been investigated successively. The results indicated that reflection-asymmetric deformation plays a significant role in understanding the ground-state features of these nuclei. Besides nuclei near the lanthanides and actinides, the ground-state properties and possible octupole deformations for Sr, Zr, Mo, and Ru isotopes have also been recently systematically researched in Ref. [83] by the RASRMF theory. It is noteworthy that although no octupole-deformed ground states are found around the traditional octupole magic numbers $N=34$ and $N=56$ in the studied isotopic chains, the possible octupole-deformed nuclei are predicted in the region near $N=40$, consistent with the results from both nonrelativistic Hartree-Fock-Bogoliubov and relativistic Hartree-Bogoliubov calculations. These findings not only effectively verify the power of the RASRMF theory for studying octupole-deformed nuclei in traditional regions but also exhibit its potential for exploring new octupole deformation regions.

As noted previously, current theoretical and experimental investigations of octupole-deformed nuclei primarily focus on mass regions where neutron and/or proton numbers are around the octupole magic numbers (34, 56, 88, and 134), especially in neutron-rich lanthanides with $(N,Z)\approx(88,56)$ and neutron-deficient actinides with $(N,Z)\approx(134,88)$. However, in addition to investigating octupole-related features of atomic nuclei in the traditional regions, the search for new octupole deformation regions across the entire nuclide chart has also emerged as an active frontier in contemporary nuclear structure physics.

Möller *et al*. [84] systematically investigated ground-state deformations in 9318 nuclei from ^{16}O to $A=339$ based on the MM model, revealing an island of octupole deformation centered at $Z\approx100$, $N\approx184$. The global survey of ground-state octupole deformation for even-even nuclei with $Z\leq106$ located between the two-neutron and two-proton driplines using the DD-PC1 [85] and NL3* [86] EDFs was carried out in Ref. [87]. In particular, this work predicted, for the first time, a new region of octupole-deformed nuclei centered at $Z\approx98$, $N\approx196$. Similarly, Cao *et al*. [88] performed systematic calculations of octupole shapes for even-even nuclei with $Z\leq110$ and $N\leq210$ employing five Skyrme (UNEDF0 [89], UNEDF1 [90], UNEDF2 [91], SLy4 [92], and SV-min [93]) and four relativistic EDFs (NL3*, DD-PC1, DD-ME2 [94], and PC-PK1 [95]). Their calculations show that reflection-asymmetric shapes exist in numerous neutron-rich actinide and transactinide nuclei with $184<N<206$. Beyond the global analyses, there are also dedicated investigations of ground-state octupole deformation for neutron-rich actinides and superheavy nuclei [67, 96−98], which encompass nuclides inaccessible to new-generation radioactive beam facilities. For example, the MM calculations in Ref. [97] for the nuclei with $98\leq Z\leq126$ and $134\leq N\leq192$ revealed a region of octupole-deformed nuclei at $Z\approx102$ and $N\approx188$. Additionally, octupole correlations in the nuclei with $92\leq Z\leq110$ and $186\leq N\leq202$ have been studied in Ref. [98] based on the Gogny-D1M [99] EDF, and static octupole deformations have been predicted around $N=192$. All these approaches predict the existence of an island of octupole deformation in neutron-rich actinides and low-Z superheavy nuclei. Notably, while the island's center remains consistently around $Z=100$, the corresponding neutron number exhibits significant discrepancies across different models. Given the recurring interest in searching for new regions of octupole-deformed nuclei, it is meaning-

ful to conduct a systematic theoretical analysis of the octupole properties in the ground state of neutron-rich nuclei with $Z \approx 100$.

To gain deeper insights into octupole deformation of neutron-rich nuclei around $Z = 100$ and examine its effect on nuclear properties, we employ the RASRMF theory to systematically analyze the ground-state properties of $^{268-308}$Cf ($Z = 98$), $^{270-310}$Fm ($Z = 100$), $^{272-312}$No ($Z = 102$), and $^{274-314}$Rf ($Z = 104$) isotopes. Furthermore, the critical role of the Coulomb interaction in characterizing the ground-state properties of neutron-rich actinides and low-Z superheavy nuclei is evaluated. The paper is organized as follows: Sec. II provides an overview of the RASRMF theory, Sec. III presents the numerical details and results, and Sec. IV offers a summary of the findings.

II. THEORETICAL FRAMEWORK

To explore the ground-state properties and possible octupole deformations of neutron-rich nuclei with $98 \le Z \le 104$, we first present the theoretical formalism of RASRMF. The starting point of the RASRMF theory is an effective Lagrangian density [61−64],

$$\begin{aligned}\mathcal{L} = &\bar{\psi}[i\gamma^{\mu}\partial_{\mu} - M - g_{\sigma}\sigma - g_{\omega}\omega_{\mu}\gamma^{\mu} - g_{\rho}\vec{\rho}_{\mu}\vec{\tau}\gamma^{\mu} \\ &- \frac{1}{2}e\gamma^{\mu}(1-\tau_3)A_{\mu}]\psi + \frac{1}{2}(\partial_{\mu}\sigma\partial^{\mu}\sigma - m_{\sigma}^2\sigma^2) \\ &- \frac{1}{4}\omega^{\mu\nu}\omega_{\mu\nu} + \frac{1}{2}m_{\omega}^2\omega^{\mu}\omega_{\mu} - \frac{1}{3}g_2\sigma^3 - \frac{1}{4}g_3\sigma^4 \\ &- \frac{1}{4}\vec{\rho}^{\mu\nu}\vec{\rho}_{\mu\nu} + \frac{1}{2}m_{\rho}^2\vec{\rho}^{\mu}\vec{\rho}_{\mu} + \frac{1}{4}c_3(\omega^{\mu}\omega_{\mu})^2 - \frac{1}{4}A^{\mu\nu}A_{\mu\nu}, \end{aligned} \quad (1)$$

where ψ is the Dirac spinor of the nucleon with the corresponding mass M, σ is the isoscalar-scalar meson that provides medium-range attraction, ω is the isoscalar-vector meson that provides short-range repulsion, ρ is the isovector-vector meson reflecting the difference between the neutron and proton, and A is the photon field describing the electromagnetic properties of atomic nuclei. m_{σ}, m_{ω}, and m_{ρ} are the masses of the σ, ω, and ρ mesons. g_{σ}, g_{ω}, and g_{ρ} are the coupling constants of the mesons with the nucleons. g_2, g_3, and c_3 are the nonlinear self-coupling coefficients of the σ and ω mesons. Since the c_3 parameter is absent from the NL3 [100] and NL3* effective interactions, it was set to zero in the corresponding calculations. The field tensors for the mesons and photons are defined as

$$\begin{aligned}\omega^{\mu\nu} &= \partial^{\mu}\omega^{\nu} - \partial^{\nu}\omega^{\mu}, \\ \vec{\rho}^{\mu\nu} &= \partial^{\mu}\vec{\rho}^{\nu} - \partial^{\nu}\vec{\rho}^{\mu}, \\ A^{\mu\nu} &= \partial^{\mu}A^{\nu} - \partial^{\nu}A^{\mu}.\end{aligned}$$

Starting from the Lagrangian density, using the classical variational principle, one can derive the Dirac equation for the nucleons,

$$[-i\vec{\alpha}\cdot\vec{\nabla} + V(\vec{r}) + \beta(M + S(\vec{r}))]\psi_i = \epsilon_i\psi_i, \quad (2)$$

with the scalar potential $S(\vec{r})$ and vector potential $V(\vec{r})$

$$\begin{aligned}S(\vec{r}) &= g_{\sigma}\sigma(\vec{r}), \\ V(\vec{r}) &= g_{\omega}\omega_0(\vec{r}) + g_{\rho}\tau_3\rho_0(\vec{r}) + e\frac{(1-\tau_3)}{2}A_0(\vec{r}),\end{aligned} \quad (3)$$

and the Klein-Gordon equations for the mesons and photons,

$$\begin{aligned}\left(-\Delta + m_{\sigma}^2\right)\sigma &= -g_{\sigma}\rho_s - g_2\sigma^2 - g_3\sigma^3, \\ \left(-\Delta + m_{\omega}^2\right)\omega_0 &= g_{\omega}\rho_v - c_3\omega_0^3, \\ \left(-\Delta + m_{\rho}^2\right)\rho_0 &= g_{\rho}\rho_3, \\ -\Delta A_0 &= e\rho_c,\end{aligned} \quad (4)$$

with the densities

$$\begin{aligned}\rho_s &= \sum_{i=1}^{A}\bar{\psi}_i\psi_i, \rho_v = \sum_{i=1}^{A}\psi_i^{\dagger}\psi_i, \\ \rho_3 &= \sum_{i=1}^{A}\psi_i^{\dagger}\tau_3\psi_i, \rho_c = \sum_{p=1}^{Z}\psi_p^{\dagger}\psi_p.\end{aligned} \quad (5)$$

Solving Eqs. (2)−(5) iteratively, we can obtain the single-particle energies, wave functions, densities, fields, and nuclear binding energies. Equations (2) and (4) are nonlinear coupled equations and are solved by the basis expansion method. For axially symmetric deformed nuclei, the Dirac spinors can be presented as

$$\begin{aligned}\psi_i(\vec{r},t) &= \begin{pmatrix} f_i(\vec{r},s,t) \\ ig_i(\vec{r},s,t) \end{pmatrix} \\ &= \frac{1}{\sqrt{2\pi}}\begin{pmatrix} f_i^{+}(z,r_{\perp})e^{i(\Omega_i-\frac{1}{2})\varphi} \\ f_i^{-}(z,r_{\perp})e^{i(\Omega_i+\frac{1}{2})\varphi} \\ ig_i^{+}(z,r_{\perp})e^{i(\Omega_i-\frac{1}{2})\varphi} \\ ig_i^{-}(z,r_{\perp})e^{i(\Omega_i+\frac{1}{2})\varphi} \end{pmatrix}\chi_{t_i}(t),\end{aligned} \quad (6)$$

where Ω_i is the third component of angular momentum. To include the reflection-asymmetric degree of freedom, the eigenfunctions of the TCHO potential are used as the basis to expand the Dirac spinors $f_i^{\pm}$ and $g_i^{\pm}$ in the RMF calculations.

The TCHO potential was initially adopted by the Frankfurt research group to construct the two-center shell

model [101, 102]. The model has subsequently been widely applied in research on fission, fusion, heavy-ion emission, and various cluster phenomena [103]. In recent years, the TCHO basis has also been introduced in the MM model [104] as well as in the relativistic and nonrelativistic density functional theory [28, 105−111]. It has proven particularly suitable for describing the reflection-asymmetric shape and fission of atomic nuclei. The TCHO potential [76] has the following form:

$$V(r_\perp,z)=\frac{1}{2}M\omega_\perp^2 r_\perp^2+\begin{cases}\frac{1}{2}M\omega_1^2(z+z_1)^2, & z<0,\\ \frac{1}{2}M\omega_2^2(z-z_2)^2, & z\geq 0.\end{cases} \tag{7}$$

Here, z_1 and z_2 represent the distances from the centers of the ellipsoids to the plane of their intersection, and ω_1 (ω_2) corresponds to the oscillation frequency of the harmonic oscillator for $z<0$ ($z\geq 0$). The eigenfunction of the TCHO potential can be obtained by solving the Schrödinger equation in the cylindrical coordinate system, and it can be written as

$$\Phi(r_\perp,z,\varphi,s)=\phi_{n_r}^{m_l}(r_\perp)\phi_\nu(z)\Theta(\varphi)\chi_{m_s}(s), \tag{8}$$

with

$$\phi_{n_r}^{m_l}(r_\perp)=\frac{\sqrt{2}}{b_\perp}\sqrt{\frac{n_r!}{(n_r+m_l)!}}\eta^{m_l/2}L_{n_r}^{m_l}(\eta)e^{-\eta/2},$$

$$\phi_\nu(z)=\begin{cases}C_{\nu_1}H_{\nu_1}(-\zeta_1)e^{-\zeta_1^2/2}, & z<0,\\ C_{\nu_2}H_{\nu_2}(\zeta_2)e^{-\zeta_2^2/2}, & z\geq 0,\end{cases}$$

$$\Theta(\varphi)=\frac{1}{\sqrt{2\pi}}e^{im_l\varphi}.$$

Where $L_{n_r}^{m_l}(\eta)$ and $H_\nu(\zeta)$ represent the Laguerre polynomial and Hermite function, respectively. Moreover, $\eta=r_\perp^2/b_\perp^2$, $\zeta_1=(z+z_1)/b_1$, and $\zeta_2=(z-z_2)/b_2$. $b_\perp$, b_1, and b_2 are the characteristic lengths of the harmonic oscillator, and $C_{\nu_i}(i=1,2)$ is the normalization constant (see Ref. [112] for full details).

The TCHO basis can be completely determined by the following three parameters: δ_2, δ_3, and Δz. δ_2 is the quadrupole deformation parameter in the hemisphere with $z>0$. δ_3 is the asymmetric coefficient of the TCHO basis, $\delta_3=\omega_1/\omega_2$. When $\delta_3=1$, the system is reflection symmetric. Δz ($=z_1+z_2$) represents the center distance of the TCHO basis. Here, we mainly focus on the reflection-asymmetric deformation of atomic nuclei, and the adopted Δz is consistent with that in Ref. [76].

Using Eq. (8), we expand the upper and lower components of the Dirac spinor as

$$f_i(\vec{r},s,t)=\frac{1}{\sqrt{2\pi}}\begin{pmatrix}f_i^+(z,r_\perp)e^{i(\Omega-\frac{1}{2})\varphi}\\ f_i^-(z,r_\perp)e^{i(\Omega+\frac{1}{2})\varphi}\end{pmatrix}=\sum_\alpha^{\alpha_{\max}}f_\alpha^{(i)}\Phi_\alpha(\vec{r},s)\chi_{t_i}(t),$$
$$g_i(\vec{r},s,t)=\frac{1}{\sqrt{2\pi}}\begin{pmatrix}g_i^+(z,r_\perp)e^{i(\Omega-\frac{1}{2})\varphi}\\ g_i^-(z,r_\perp)e^{i(\Omega+\frac{1}{2})\varphi}\end{pmatrix}=\sum_{\tilde{\alpha}}^{\tilde{\alpha}_{\max}}g_{\tilde{\alpha}}^{(i)}\Phi_{\tilde{\alpha}}(\vec{r},s)\chi_{t_i}(t). \tag{9}$$

The Dirac equation can be correspondingly written in matrix form,

$$\begin{pmatrix}A_{\alpha,\alpha'} & B_{\alpha,\tilde{\alpha}'}\\ B_{\tilde{\alpha},\alpha'} & -C_{\tilde{\alpha},\tilde{\alpha}'}\end{pmatrix}\begin{pmatrix}f_{\alpha'}^{(i)}\\ g_{\tilde{\alpha}'}^{(i)}\end{pmatrix}=\epsilon_i\begin{pmatrix}f_\alpha^{(i)}\\ g_{\tilde{\alpha}}^{(i)}\end{pmatrix}. \tag{10}$$

By diagonalizing the Hamiltonian matrix above, which has dimensions $\alpha_{\max}+\tilde{\alpha}_{\max}$, we can obtain the single-particle energies and wave functions.

III. RESULTS AND DISCUSSION

Based on the aforementioned formalism, we delve into the octupole properties in the ground states of Cf, Fm, No, and Rf isotopes with $170\leq N\leq 210$. In the present calculations, the NL3, NL3*, and PK1 [113] parameter sets are adopted. Since these three interactions yield consistent conclusions, only the results obtained with the NL3 interaction are shown here for clarity. To ensure convergence for the studied physical quantities, 20 major shells are considered in the TCHO basis. The pairing correlations are treated using the BCS approximation with a constant pairing gap. For convenience, an empirical formula $\Delta=12/\sqrt{A}$ [114] is employed for the neutron and proton pairings.

The binding energies per nucleon E/A for the Cf, Fm, No, and Rf isotopes as a function of the neutron number N are depicted in Fig. 1. The red circles denote the specific binding energies from the RASRMF calculations, while the black squares represent the results from the usual reflection-symmetric relativistic mean-field (RSRMF) calculations for a clearer understanding of the impact of the reflection-asymmetric degree of freedom on the binding energies of these nuclei. In Fig. 2, we present the energy difference between RSRMF and RASRMF calculations. As shown in Fig. 1, the binding energies decrease gradually with the increasing neutron number across all isotopic chains in both the RSRMF and RASRMF calculations. When reflection asymmetry is considered, the binding energies of Cf, Fm, No, and Rf isotopes around $N=184$ and $N=196$ show a pronounced gain relative to the RSRMF results, which enhances the stability of the nuclear ground state. This gain in binding energy also im-

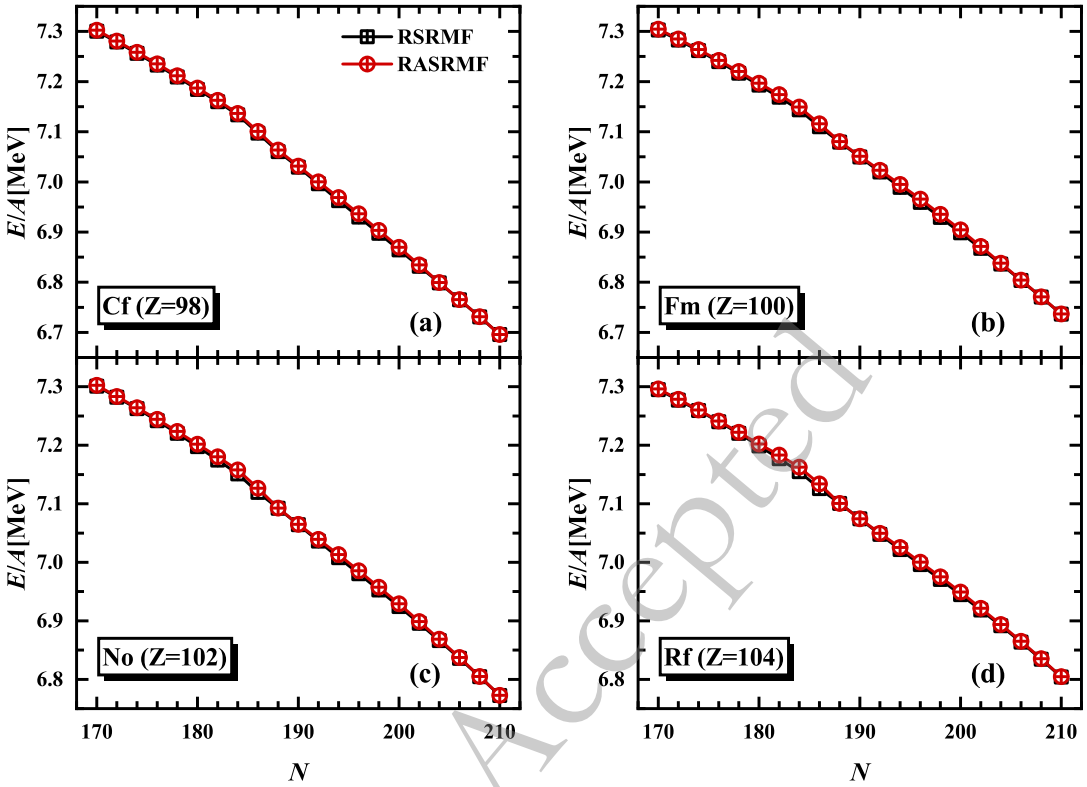

Fig. 1. (color online) Binding energy per nucleon E/A and its variation with the neutron number N in the (a) Cf, (b) Fm, (c) No, and (d) Rf isotopes. The black squares represent the results obtained from the RSRMF calculations, while the red circles correspond to those obtained from the RASRMF calculations.

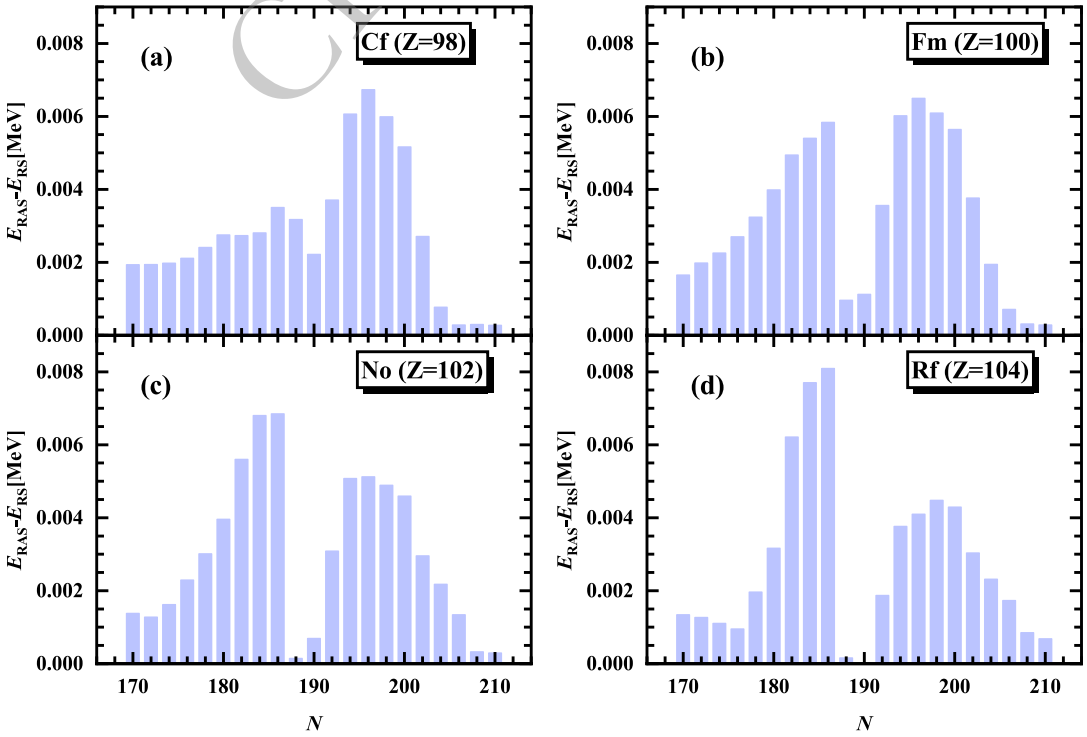

Fig. 2. (color online) The difference between the binding energy per nucleon of the (a) Cf, (b) Fm, (c) No, and (d) Rf isotopes obtained from the RSRMF and RASRMF calculations.

plies the possible presence of octupole deformations in the ground states of these nuclei, as seen in Fig. 4. Furthermore, as the proton number increases from $Z = 98$ to $Z = 104$, the energy gain around $N = 184$ caused by the octupole deformation progressively rises. For the isotopes in the vicinity of $N = 174$ and $N = 206$, the RASRMF calculations nearly match the RSRMF calculations, indicating that octupole deformation has little effect on the binding energies of these nuclei.

The nuclear shape is one of the most fundamental properties of nuclei. By introducing the reflection-asymmetric degree of freedom, the RASRMF theory can simultaneously provide the ground-state quadrupole and octupole deformations of atomic nuclei.

In Fig. 3, we display the quadrupole deformation β_{20} of Cf, Fm, No, and Rf isotopes as obtained from the RSRMF and RASRMF calculations. It can be clearly seen that along all these isotopic chains, both calculations present a consistent trend of deformation evolution, i.e., an initial decrease followed by an increase. However, due to the inclusion of the reflection-asymmetric degree of freedom, the β_{20} values calculated by RASRMF show some deviations from those calculated by RSRMF. Specifically, for those isotopes near the neutron magic number $N = 184$, RSRMF predicts the ground states with $\beta_{20} \approx 0$, whereas RASRMF generally yields slightly larger quadrupole deformations. A similar scenario also occurs in the $190 < N < 196$ region of Cf, Fm, No, and Rf isotopic chains, where the RASRMF calculations give enhanced β_{20} values compared to the RSRMF calculations. Conversely, after $N = 196$, RASRMF predicts smaller deformations than RSRMF, up to $N = 204$. For the extremely neutron-rich region with $N > 204$, the difference between the RASRMF and RSRMF calculations increases gradually from Cf ($Z = 98$) to Rf ($Z = 104$) isotopes. Furthermore, for the nuclei with $N \approx 172$, the quadrupole deformations obtained from both calculations are consistent.

To explore the possible region of octupole deformation for neutron-rich nuclei with $Z \approx 100$, Fig. 4 presents the predicted octupole deformation β_{30} and its evolution with the neutron number N in Cf, Fm, No, and Rf isotopes. The obtained β_{30} by the RSRMF calculations is zero for all isotopic chains due to the absence of the octupole degree of freedom. In contrast, the ground states of the majority of atomic nuclei for these chains are predicted to have nonzero octupole deformations in the RASRMF calculations. As can be seen from Figs. 4(a) and 4(b), nonzero β_{30} values exist in both Cf and Fm isotopes with $N = 170 - 206$. Particularly, $|\beta_{30}| \leq 0.1$ in the range of $170 \leq N \leq 188$, while $|\beta_{30}| > 0.1$ in the range of $190 \leq N \leq 204$. From Figs. 4(c) and 4(d), we observe that the ground states of the No isotopes with $174 \leq N \leq 186$ and $190 \leq N \leq 206$, as well as the Rf isotopes with

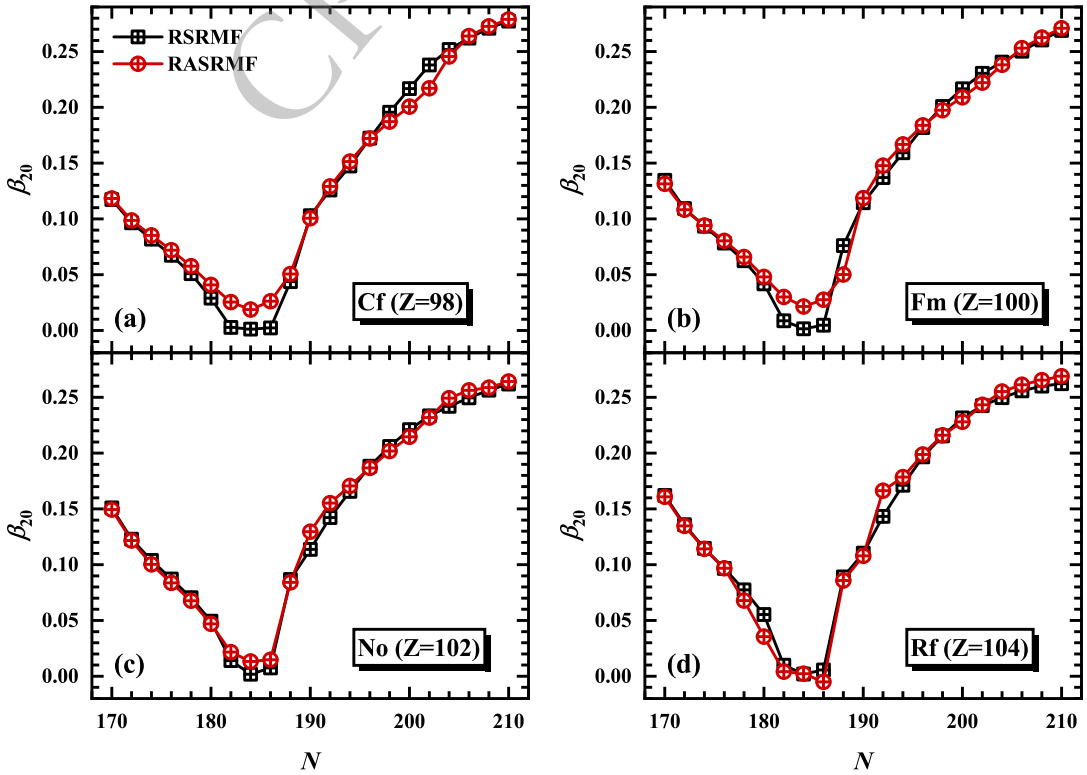

Fig. 3. (color online) The quadrupole deformation β_{20} for the (a) Cf, (b) Fm, (c) No, and (d) Rf isotopes obtained from the RSRMF (black squares) and RASRMF (red circles) calculations as a function of the neutron number N.

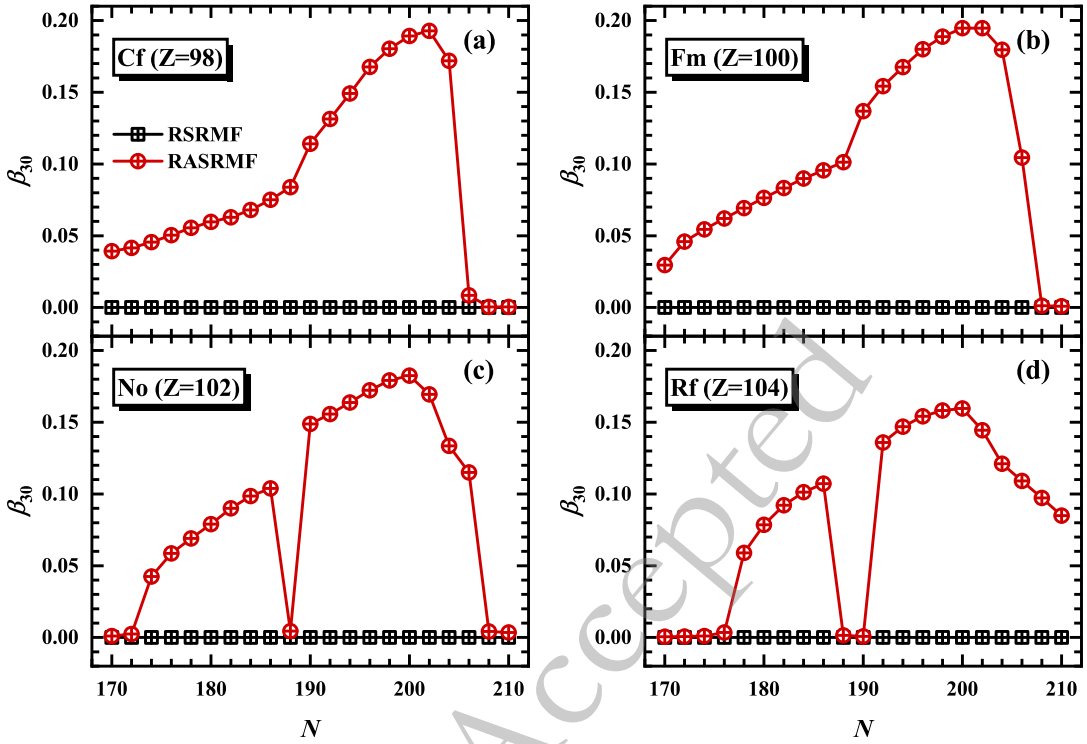

Fig. 4. (color online) The octupole deformation β_{30} for the (a) Cf, (b) Fm, (c) No, and (d) Rf isotopes as a function of the neutron number N. The black squares and red circles represent the results from the RSRMF and RASRMF calculations, respectively.

$178 \le N \le 186$ and $192 \le N \le 210$, are octupole-deformed. Furthermore, a pronounced change occurs in the β_{30} value of the No and Rf isotopes around $N = 188$, whereas such a change is absent in the Cf and Fm isotopes. By performing constrained RASRMF calculations for ^{290}No, ^{292}Rf, and ^{294}Rf, we found that this variation may arise from the presence of coexistence of prolate and pear shapes within these nuclei. Overall, the predicted octupole-deformed nuclei concentrate predominantly in the vicinity of neutron numbers $N = 184$ and $N = 196$ in all the studied isotopes, and the β_{30} values near $N = 196$ are universally larger than those near $N = 184$. Similar results, not shown here, have also been obtained from RASRMF calculations employing both the NL3* and PK1 parameter sets. It is worth noting that the present calculations are consistent with the nonrelativistic Hartree-Fock-Bogoliubov (HFB) calculations [88] using the UNEDF1 and UNEDF2 functionals, but do not completely agree with the MM calculations [84] and the relativistic Hartree-Bogoliubov (RHB) calculations [87] with the NL3* functional. The MM and RHB calculations only predict nonzero β_{30} values around $N = 184$ and $N = 196$, respectively. For neutron-rich isotopes around $Z = 100$, although there are differences between the predictions of various models for the range of octupole-deformed nuclei, the obtained nonzero octupole deformations are mainly located around $N = 184$ and/or $N = 196$, which indicates that the RASRMF results should be reliable.

Recently, Tarasov *et al.* [115] examined the dependence of octupole deformation in nuclei on the strength of the pairing interaction. The results indicate that increasing the pairing force can lead to a reduction or even the complete disappearance of octupole deformation in nuclei. To confirm this assertion, we explore the effect of variations in the pairing gap on the octupole deformation of nuclei in Fig. 5, using Fm isotopes as an illustrative example. One can clearly see that, as the pairing parameter δ increases from 10 to 14, the octupole deformations decrease accordingly for the considered nuclei. Additionally, the ground-state octupole deformation of Fm isotopes with $N \approx 184$ is more sensitive to the change in the pairing gap than that of Fm isotopes with $N \approx 196$. These findings are consistent with previous studies [115–117] that highlight the role of pairing interactions in the octupole deformation of nuclei. In particular, the appropriate selection of the pairing gap is essential for achieving an accurate prediction of octupole deformation in nuclei in calculations employing the BCS approximation with a constant pairing gap.

As another fundamental property of atomic nuclei, the nuclear radius is a crucial observable that directly reflects various exotic nuclear phenomena and is sensitive to deformation effects. To illustrate the role of octupole deformation in the nuclear radii, the root-mean-square (rms) radii of neutrons and protons as well as the charge radii as a function of the neutron number N for the Cf, Fm, No, and Rf isotopes obtained by the RSRMF and

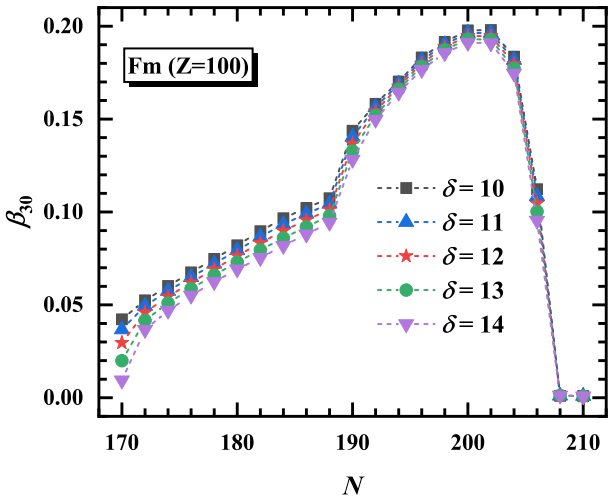

Fig. 5. (color online) The octupole deformation β_{30} of Fm isotopes obtained from the RASRMF calculations with different values of the pairing parameter δ. The empirical pairing gap is given by $\Delta = \delta/\sqrt{A}$.

RASRMF calculations are plotted in Figs. 6, 7, and 8, respectively. From Fig. 6, it can be seen that the neutron radii for each isotopic chain exhibit a smooth evolution trend with the increasing neutron number in both calculations. For the nuclei with the neutron number below $N = 190$ in all isotopic chains, the neutron radii obtained in the RASRMF calculations are consistent with those obtained in the RSRMF calculations, implying that the impact of octupole deformation on the neutron radii of these nuclei is negligible. As Fig. 4 elucidates, the majority of the nuclei with $N < 190$ exhibit nonzero octupole deformation. Additionally, for the very neutron-rich nuclei around $N = 196$, RASRMF predicts larger R_n compared to those by the RSRMF calculations due to the significant octupole deformation effects. Similar to Fig. 6, the calculated proton and charge radii present a smooth evolution along these chains in Figs. 7 and 8, respectively. With the incorporation of the octupole degree of freedom in RASRMF, larger proton and charge radii are observed in the ground states of Cf, Fm, No, and Rf isotopes around $N = 196$. Notably, the additional increase in R_p and R_c also appears in these isotopes around $N = 184$, and the amplitude of increase grows more pronounced with the proton number. It can also be observed that the deviation between the RSRMF and RASRMF calculations, arising from the octupole deformation effects, in the proton and charge radii is more marked than that in the neutron radii. This suggests that the proton and charge radii are more sensitive to octupole deformation than the neutron radii in the studied nuclei.

The binding energies, deformations, and radii of Cf, Fm, No, and Rf isotopes with $170 \le N \le 210$, obtained through detailed studies, have emphasized the significant

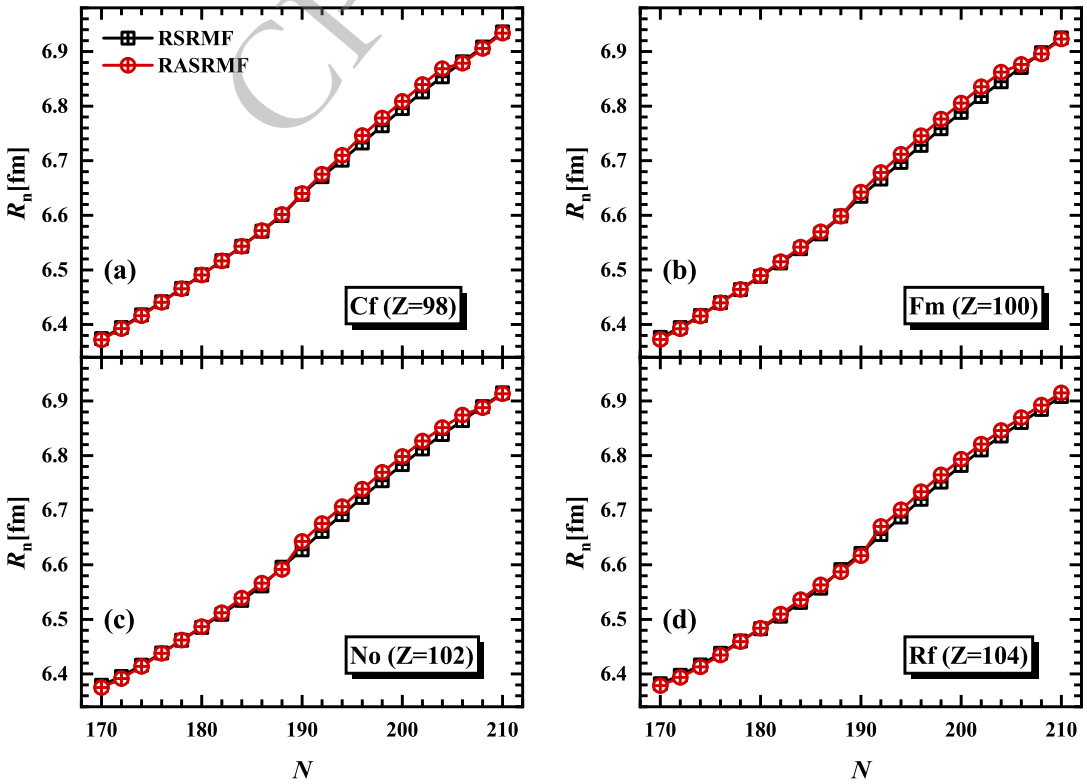

Fig. 6. (color online) Neutron rms radius R_n for the (a) Cf, (b) Fm, (c) No, and (d) Rf isotopes as a function of the neutron number N. The RSRMF and RASRMF results are shown by black squares and red circles, respectively.

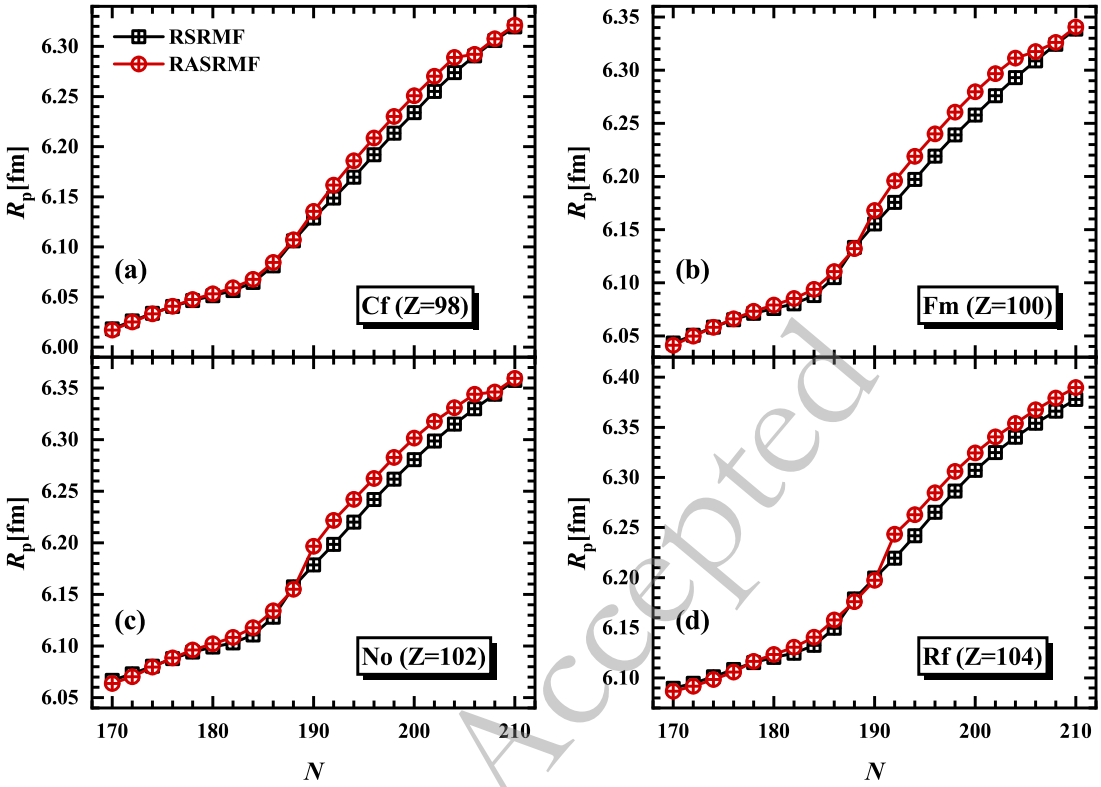

Fig. 7. (color online) Same as Fig. 6, but for the proton rms radius R_p.

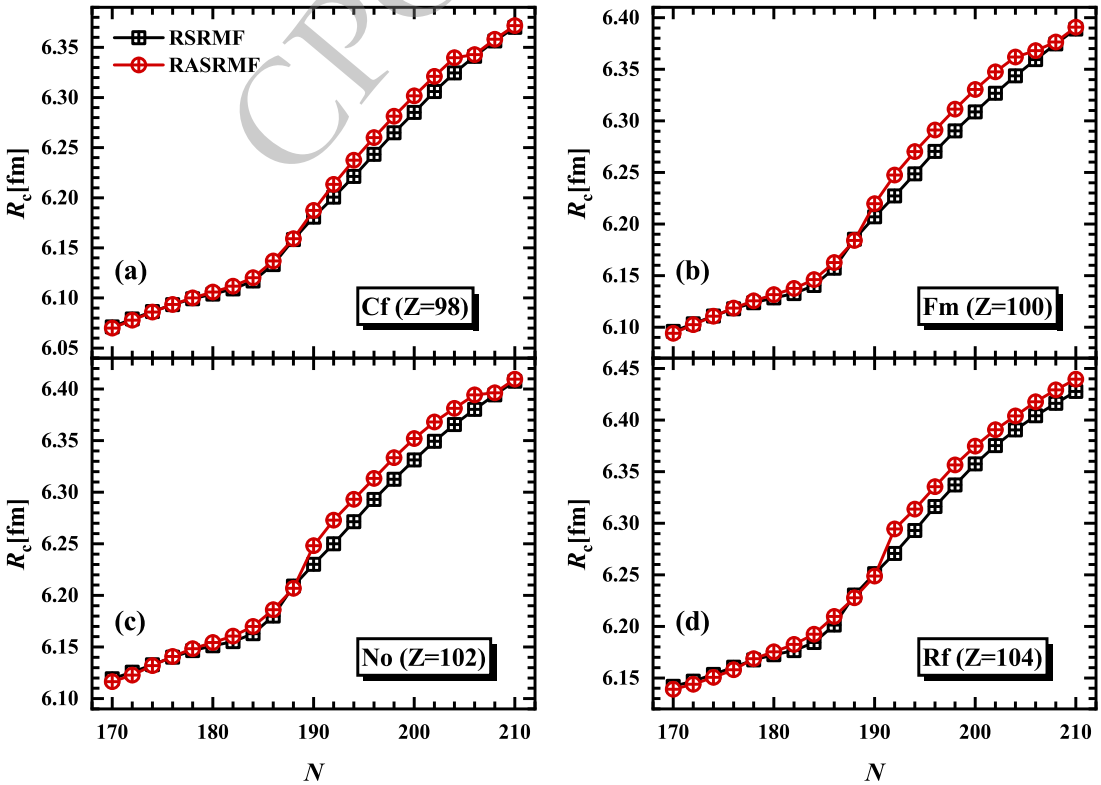

Fig. 8. (color online) Same as Fig. 6, but for the charge radius R_c.

role of the reflection-asymmetric degree of freedom in describing the ground-state properties of neutron-rich actinides and low-Z superheavy nuclei. Recently, the influence of the Coulomb interaction on the nuclear properties was investigated in Ref. [118]. It was found that the Coulomb interaction enhances the quadrupole deformation across a broad range of nuclei. However, this study was restricted to even-even nuclei with $2 \le Z \le 60$, which has sparked our interest in examining the extent to which the ground-state properties of neutron-rich nuclei with $Z \approx 100$ are affected by the Coulomb interaction.

The binding energies per nucleon E/A, quadrupole deformations β_{20}, octupole deformations β_{30}, neutron radii R_n, proton radii R_p, and charge radii R_c for the Cf, Fm, No, and Rf isotopes obtained in the RASRMF calculations without and with the Coulomb interaction are presented in Figs. 9, 10, 11, 12, 13, and 14, respectively. As illustrated in Fig. 9, the specific binding energies of all the studied nuclei are dramatically reduced when the Coulomb interaction is taken into account. This lowering effect drives the ground state of these neutron-rich isotopes with the high proton number Z toward greater instability. It is also found that the influence of the Coulomb interaction on the binding energies generally decreases with the increase of the neutron number. However, due to the dependence of this influence on the neutron number being relatively weak, the isotopic trend of the binding energies is similar to that obtained when neglecting the Coulomb interaction. In Fig. 10, it can be seen that, as a general trend, the presence of the Coulomb interaction enhances the nuclear quadrupole deformation, which is consistent with previous work [118]. Especially, the increase in quadrupole deformation induced by the Coulomb interaction is more pronounced among extremely neutron-rich Cf, Fm, No, and Rf isotopes with $N \ge 190$, with the exception of ^{300}Cf ($N = 202$). In the RASRMF calculations without the Coulomb interaction, the quadrupole deformation in the Cf isotopes undergoes an abrupt rise to a larger value after $N = 200$, which compensates for the difference between both calculations at ^{300}Cf. Moreover, the magnitude of enhancement becomes relatively small in those isotopes in the vicinity of the neutron magic number $N = 184$, while the quadrupole deformations are slightly lowered by the Coulomb interaction in the isotopes near $N = 176$. In addition to the quadrupole deformation, the inclusion of the Coulomb interaction also augments the nuclear octupole deformation, which can be seen from Fig. 11. It is noted that compared to the Cf, Fm, No, and Rf isotopes with $N < 190$, the Coulomb interaction exerts a stronger influence on octupole deformation in the isotopes with $N \ge 190$. Especially for the No and Rf isotopes with

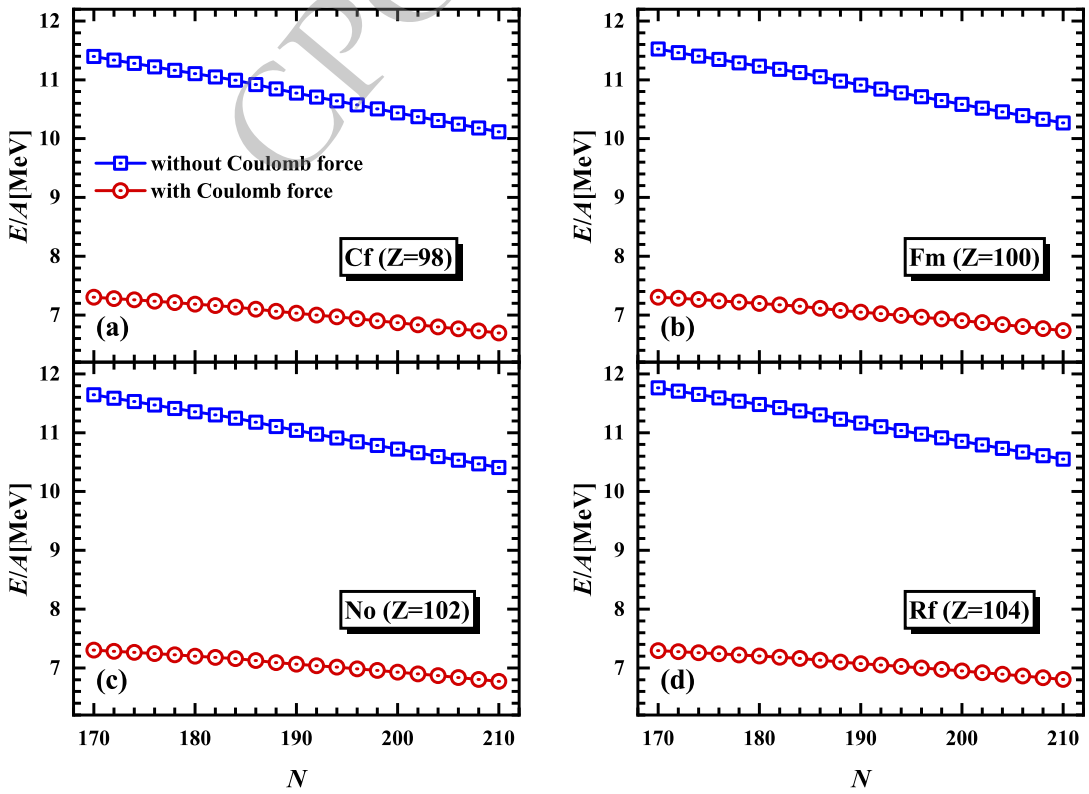

Fig. 9. (color online) Binding energy per nucleon E/A for the (a) Cf, (b) Fm, (c) No, and (d) Rf isotopes as functions of the neutron number N. The RASRMF results without and with the Coulomb interaction are shown by blue squares and red circles, respectively. The parameter set used is NL3.

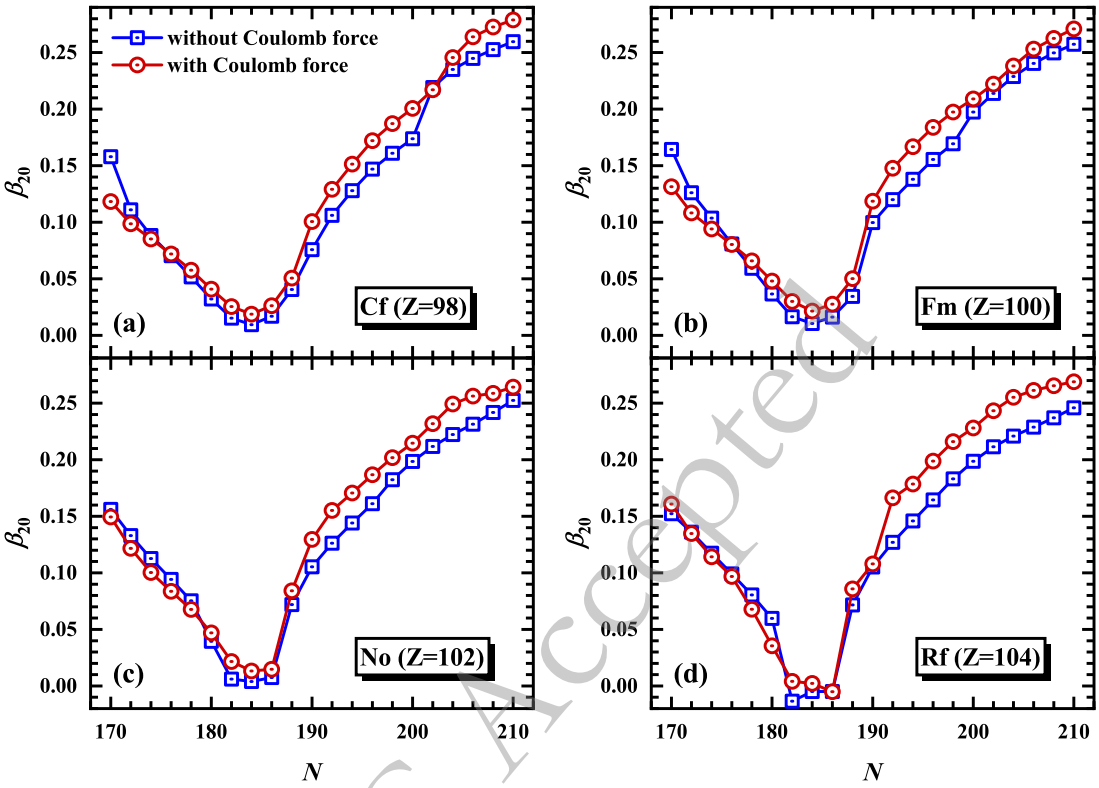

Fig. 10. (color online) Same as the caption of Fig. 9, but for the quadrupole deformation β_{20}.

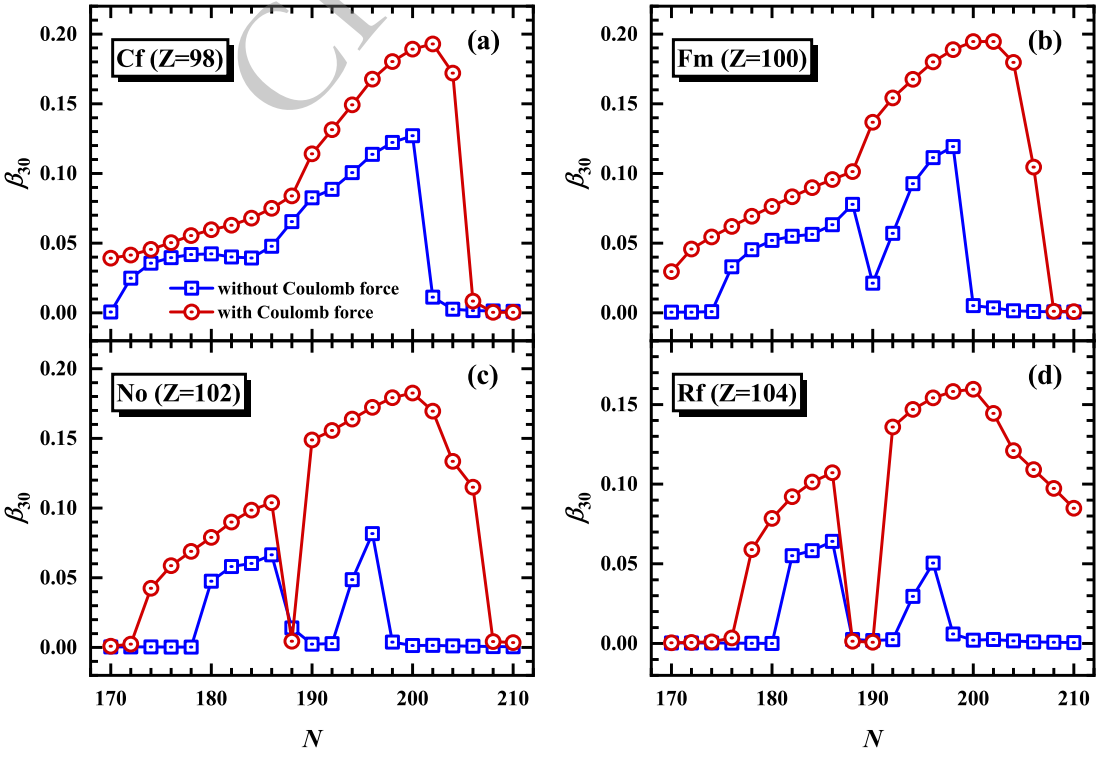

Fig. 11. (color online) Same as the caption of Fig. 9, but for the octupole deformation β_{30}.

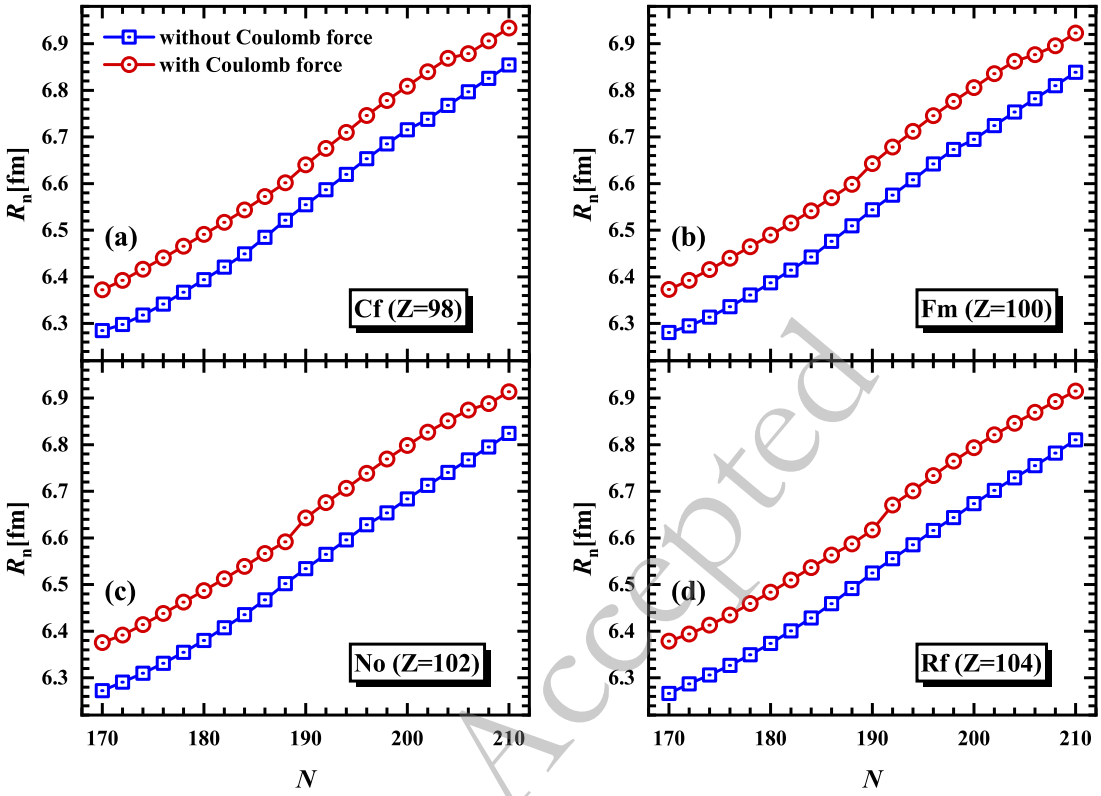

Fig. 12. (color online) Same as the caption of Fig. 9, but for the neutron rms radius R_n.

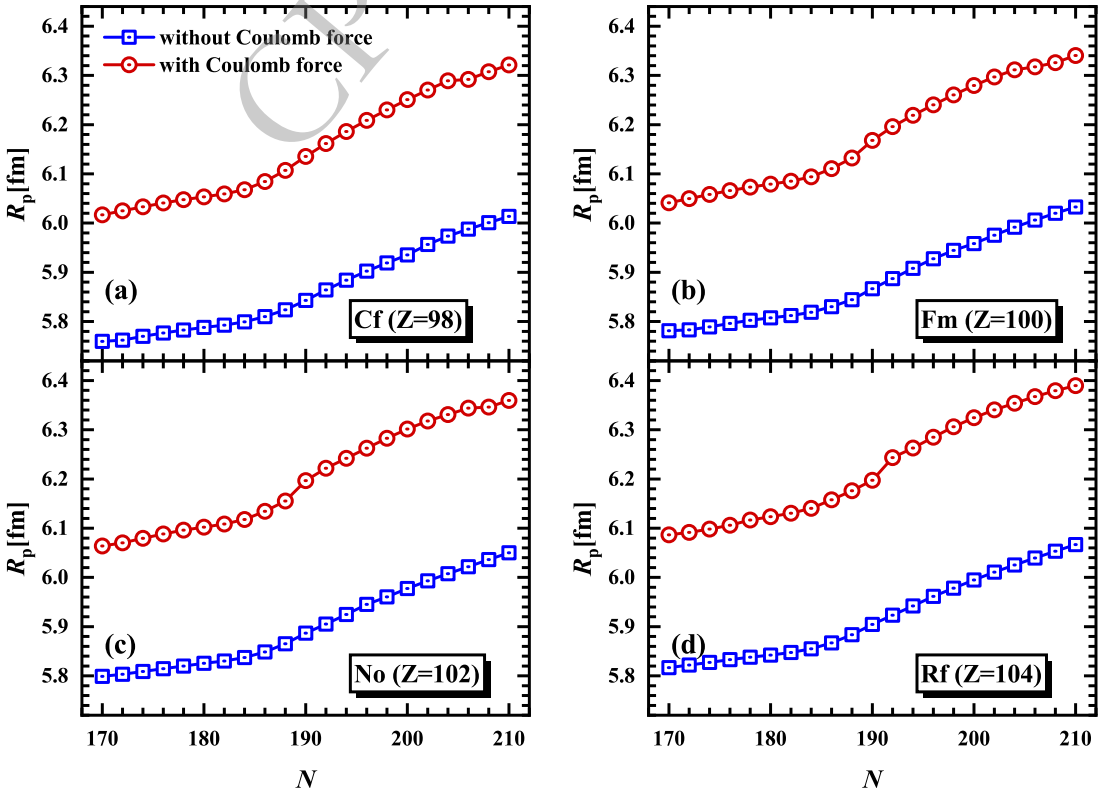

Fig. 13. (color online) Same as the caption of Fig. 9, but for the proton rms radius R_p.

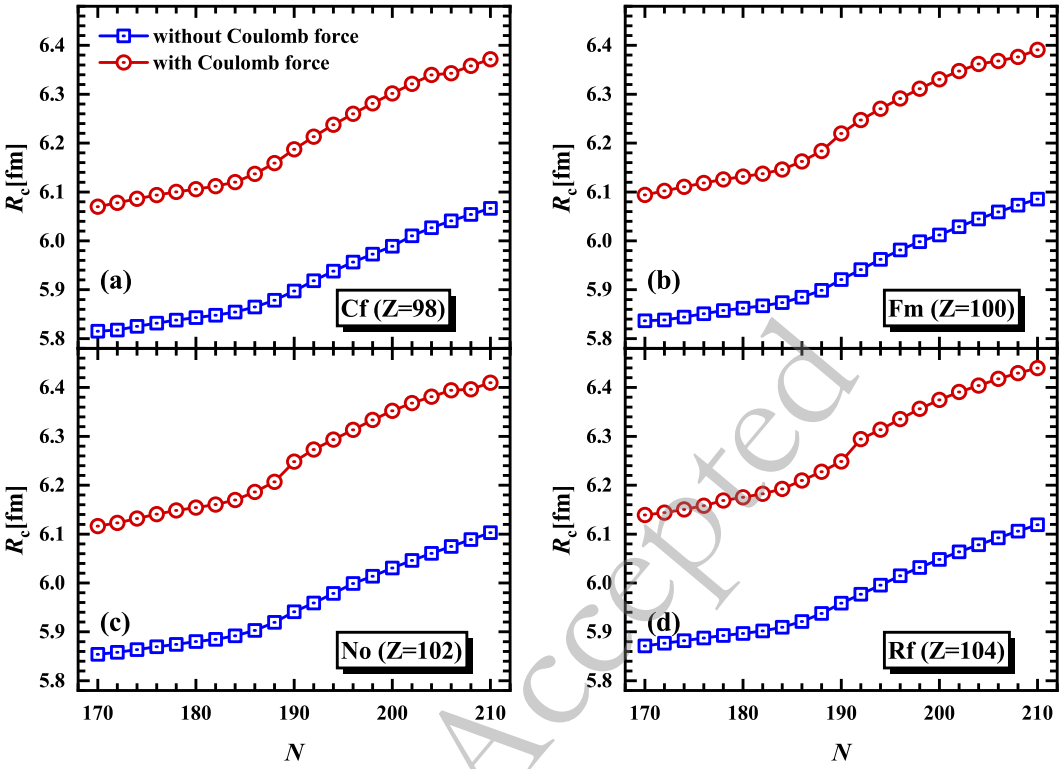

Fig. 14. (color online) Same as the caption of Fig. 9, but for the charge radius R_c.

$192 \le N \le 206$, the $|\beta_{30}|$ values calculated by the RASRMF with the Coulomb interaction are generally greater than 0.1, whereas the results obtained from the RASRMF without the Coulomb interaction are widely less than 0.1 or even zero. However, the influence of the Coulomb interaction cannot alter the overall trend of the octupole deformation with respect to the neutron number for the studied isotopic chains, which is similar to the case shown in Fig. 10. From Fig. 12, it is observed that the inclusion of the Coulomb interaction indirectly increases the nuclear neutron radii, and the radii from both calculations follow a consistent variation trend along these chains. Owing to the repulsive character of the Coulomb force between protons, as illustrated in Figs. 13 and 14, the enhancement of the proton and charge radii is more significant than that of the neutron radii. Furthermore, the proton radii gradually rise as the neutron number and proton number increase, respectively, regardless of whether the Coulomb interaction is considered. This same trend is also mirrored in the charge radii in Fig. 14.

Finally, we would like to point out that the present conclusions are robust against the parameter sets used, i.e., NL3, NL3*, and PK1, as illustrated in Fig. 15 using the Fm isotopes as an example. In addition, it is worth mentioning that nonlinear point-coupling interactions (e.g., PC-PK1, PC-X [119], and PC-L3R [120]), which avoid explicit meson degrees of freedom, have gained increasing popularity in recent years as an alternative to traditional nonlinear meson-exchange models. To further effectively take into account medium effects, various density-dependent effective interactions have also been proposed successively (e.g., DD-ME2, DD-PC1, DD-MEX [119], and DD-PCX [121]). A set of consistent results generated from various interactions is essential to reveal the underlying physics, especially the explanation for the same and different outcomes. To this end, future work should further extend the RASRMF theory to incorporate nonlinear point-coupling interactions, as well as density-dependent point-coupling and meson-exchange interactions. This will enable a more comprehensive exploration of nuclear ground-state properties and provide a broader validation of the robustness of our findings. Additionally, forthcoming work will further explore the impact of pairing force type on octupole deformation by introducing the zero-range and separable pairing forces [95, 122] into the RASRMF framework. In particular, the new interactions, e.g., PC-X, PC-L3R, DD-MEX, and DD-PCX, incorporate the separable pairing force.

IV. SUMMARY

In summary, the RASRMF theory is applied to systematically analyze the ground-state properties and possible octupole deformations for the Cf ($Z = 98$), Fm ($Z = 100$), No ($Z = 102$), and Rf ($Z = 104$) isotopes with $170 \le N \le 210$. To better understand the role of the reflection-asymmetric degree of freedom in the ground-state properties of neutron-rich actinides and low-Z super-

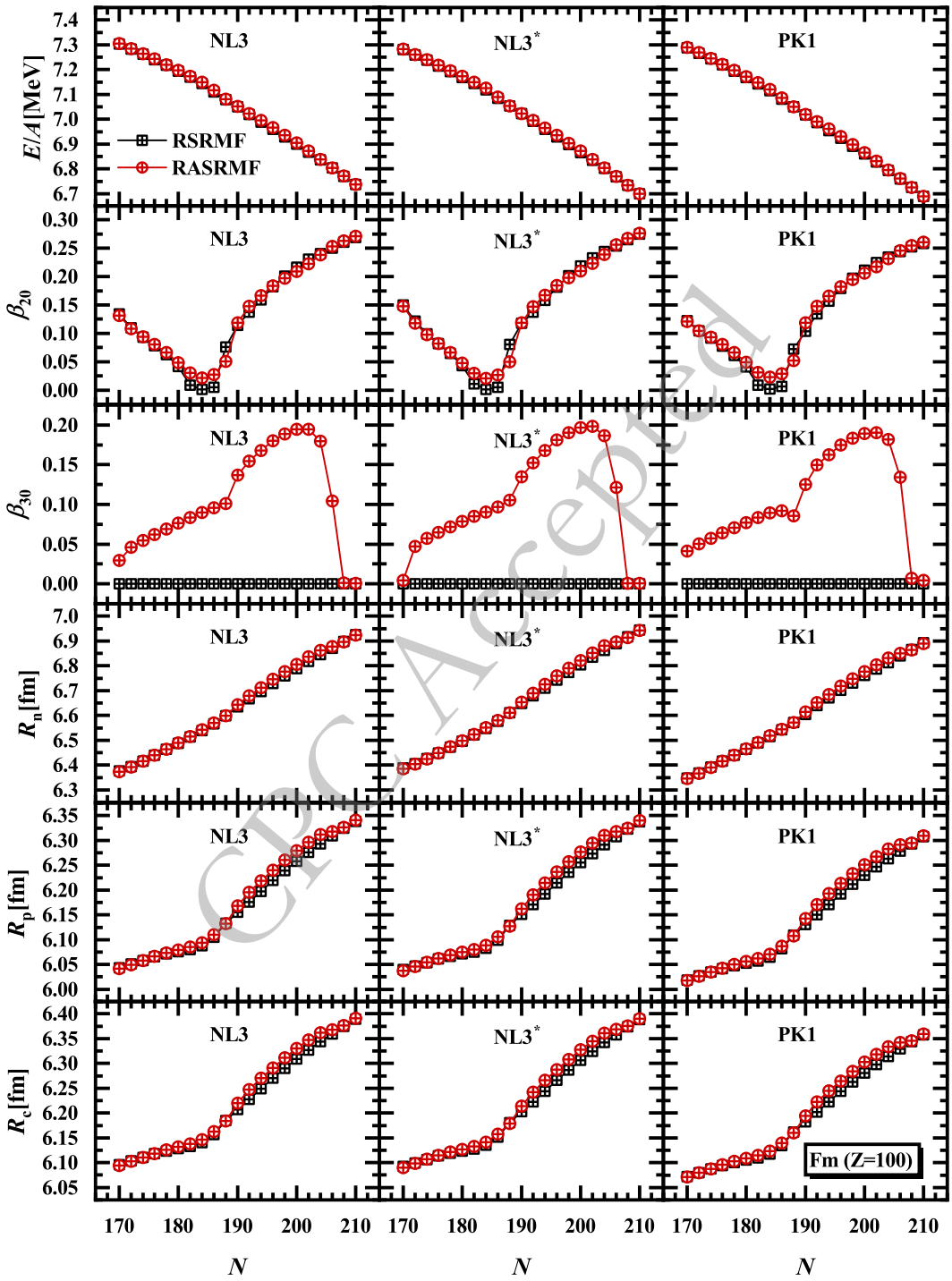

Fig. 15. (color online) The binding energy per nucleon E/A, quadrupole deformation β_{20}, octupole deformation β_{30}, neutron radius R_n, proton radius R_p, and charge radius R_c of the Fm isotopes obtained from RSRMF (black squares) and RASRMF (red circles) calculations with the NL3, NL3*, and PK1 parameter sets as a function of the neutron number N.

heavy nuclei, the results are compared to those from the RSRMF calculations. It is found that accounting for reflection asymmetry markedly enhances the binding energies of Cf, Fm, No, and Rf isotopes around $N = 184$ and $N = 196$ relative to the symmetrical case. Furthermore, across the Cf to Rf isotopes, the energy gain around $N = 184$ caused by the octupole degree of freedom progressively rises. This gain in binding energy suggests the possible existence of octupole-deformed ground states in these nuclei.

The calculated quadrupole deformation by RASRMF exhibits a few differences from the RSRMF results in the

Cf, Fm, No, and Rf isotopes, particularly in the region with $N \approx 184$ and $N \approx 196$. Although discrepancies exist in the β_{20} values due to the octupole deformation effect, both calculations follow a similar overall trend along the isotopic chains. Based on the RASRMF calculations, nonzero octupole deformations are found in the ground states of the isotopes in the vicinity of $N = 184$ and $N = 196$, with the β_{30} values near $N = 196$ generally larger than those near $N = 184$. For Cf, Fm, No, and Rf isotopes, while various models exhibit deviations in predicting the range of nuclei with nonzero β_{30}, the predicted octupole-deformed nuclei are predominantly concentrated around $N = 184$ and/or $N = 196$. This effectively validates the reliability of our results. Furthermore, the dependence of the octupole deformation on the pairing interactions is analyzed. It is found that the octupole deformation reduces with the increase of the pairing gap, suggesting that appropriately handling the pairing correlations is essential for a precise description of octupole deformation in nuclei.

The neutron, proton, and charge radii obtained by the RSRMF and RASRMF calculations present a smooth evolution trend along each isotopic chain, respectively. In particular, the inclusion of octupole deformation effects enhances the radii for the Cf, Fm, No, and Rf isotopes around $N = 184$ and $N = 196$. It is also observed that compared with the neutron radii, the deviation of the two calculations in the proton and charge radii is greater. This indicates that the proton and charge radii are more sensitive to octupole deformation than the neutron radii in the studied nuclei.

Based on the RASRMF calculations, we further examine the influence of the Coulomb interaction on the ground-state properties of the Cf, Fm, No, and Rf isotopes. It is found that the presence of the Coulomb interaction dramatically lowers the binding energies of these neutron-rich nuclei, driving their ground state toward greater instability. Moreover, the lowering effect of the Coulomb interaction systematically weakens with the increasing neutron number, but its magnitude is relatively small and insufficient to alter the evolution trend of binding energy in the studied isotopic chains. It is worth noting that, in contrast to the reduction in binding energy, the Coulomb interaction generally increases the nuclear quadrupole and octupole deformations. Particularly, the enhancement of deformation is more significant in those isotopes with $N \geq 190$ versus the Cf, Fm, No, and Rf isotopes with $N < 190$. In addition, owing to the repulsive nature of the Coulomb force between protons, the nuclear radii are also increased by the Coulomb interaction, whose impact is more pronounced on proton and charge radii than on neutron radii.

Overall, the significant deformation and Coulomb effects are verified in the ground-state properties of the studied neutron-rich actinides and low-Z superheavy nuclei. Particularly, the possible neutron octupole magic numbers $N = 184$ and 196 are predicted in the present calculations.

References

[1] K. Heyde and J. L. Wood, Rev. Mod. Phys. **83**, 1467 (2011)
[2] S. Frauendorf and J. Meng, Nucl. Phys. A **617**, 131 (1997)
[3] A. Bohr and B. R. Mottelson, Nuclear Structure, Vol. II (Benjamin, New York, 1975).
[4] N. Schunck and D. Regnier, Prog. Part. Nucl. Phys. **125**, 103963 (2022)
[5] W. Nazarewicz, P. Olanders, I. Ragnarsson, J. Dudek, G. A. Leander, P. Möller, and E. Ruchowska, Nucl. Phys. A **429**, 269 (1984)
[6] W. Nazarewicz, Nucl. Phys. A **520**, 333c (1990)
[7] P. A. Butler and W. Nazarewicz, Rev. Mod. Phys. **68**, 349 (1996)
[8] P. A. Butler, J. Phys. G **43**, 073002 (2016)
[9] P. A. Butler, Proc. R. Soc. A **476**, 20200202 (2020)
[10] S. C. Pancholi, Mod. Phys. Lett. A **36**, 2130013 (2021)
[11] L. M. Robledo and G. F. Bertsch, Phys. Rev. C **84**, 054302 (2011)
[12] K. Nomura, D. Vretenar, and B.-N. Lu, Phys. Rev. C **88**, 021303(R) (2013)
[13] W. Sun, S. Quan, Z. P. Li, J. Zhao, T. Nikšić, and D. Vretenar, Phys. Rev. C **100**, 044319 (2019)
[14] Y.-T. Rong, X.-Y. Wu, B.-N. Lu, and J.-M. Yao, Phys. Lett. B **840**, 137896 (2023)
[15] Z. K. Li and Y. Y. Wang, Nucl. Sci. Tech. **35**, 139 (2024)
[16] E. F. Zhou, X. Y. Wu, and J. M. Yao, Phys. Rev. C **109**, 034305 (2024)
[17] F. F. Xu, Y. K. Wang, Y. P. Wang, P. Ring, and P. W. Zhao, Phys. Rev. Lett. **133**, 022501 (2024)
[18] F. F. Xu, B. Li, P. Ring, and P.W. Zhao, Phys. Lett. B **856**, 138893 (2024)
[19] X. Yin, C. Ma, and Y. M. Zhao, Phys. Rev. C **109**, 024322 (2024)
[20] X. Lu, S. Jain, H. Sagawa, and S.-G. Zhou, Phys. Lett. B **868**, 139620 (2025)
[21] B.-N. Lu, E.-G. Zhao, and S.-G. Zhou, Phys. Rev. C **85**, 011301(R) (2012)
[22] N. Schunck, D. Duke, H. Carr, and A. Knoll, Phys. Rev. C **90**, 054305 (2014)
[23] R. Rodríguez-Guzmán and L. M. Robledo, Phys. Rev. C **89**, 054310 (2014)
[24] J. Zhao, J. Xiang, Z.-P. Li, T. Nikšić, D. Vretenar, and S.-G. Zhou, Phys. Rev. C **99**, 054613 (2019)
[25] X. Meng, B.-N. Lu, and S.-G. Zhou, Sci. China-Phys. Mech. Astron. **63**, 212011 (2020)
[26] Z. Li, S. Chen, Y. Chen, and Z. Li, Phys. Rev. C **106**, 024307 (2022)
[27] Z. X. Ren, D. Vretenar, T. Nikšić, P. W. Zhao, J. Zhao, and J. Meng, Phys. Rev. Lett. **128**, 172501 (2022)
[28] Y. T. Qiu and J. Y. Guo, Phys. Rev. C **109**, 044301 (2024)
[29] M. Warda and L. M. Robledo, Phys. Rev. C **84**, 044608 (2011)

[30] A. Staszczak, A. Baran, and W. Nazarewicz, Phys. Rev. C **87**, 024320 (2013)
[31] S. E. Agbemava, A. V. Afanasjev, A. Taninah, and A. Gyawali, Phys. Rev. C **99**, 034316 (2019)
[32] B. Bucher, S. Zhu, C. Y. Wu, R. V. F. Janssens, D. Cline, A. B. Hayes, M. Albers, A. D. Ayangeakaa, P. A. Butler, C. M. Campbell, M. P. Carpenter, C. J. Chiara, J. A. Clark, H. L. Crawford, M. Cromaz, H. M. David, C. Dickerson, E. T. Gregor, J. Harker, C. R. Hoffman, B. P. Kay, F. G. Kondev, A. Korichi, T. Lauritsen, A. O. Macchiavelli, R. C. Pardo, A. Richard, M. A. Riley, G. Savard, M. Scheck, D. Seweryniak, M. K. Smith, R. Vondrasek, and A. Wiens, Phys. Rev. Lett. **116**, 112503 (2016)
[33] B. Bucher, S. Zhu, C. Y. Wu, R. V. F. Janssens, R. N. Bernard, L. M. Robledo, T. R. Rodríguez, D. Cline, A. B. Hayes, A. D. Ayangeakaa, M. Q. Buckner, C. M. Campbell, M. P. Carpenter, J. A. Clark, H. L. Crawford, H. M. David, C. Dickerson, J. Harker, C. R. Hoffman, B. P. Kay, F. G. Kondev, T. Lauritsen, A. O. Macchiavelli, R. C. Pardo, G. Savard, D. Seweryniak, and R. Vondrasek, Phys. Rev. Lett. **118**, 152504 (2017)
[34] L. P. Gaffney, P. A. Butler, M. Scheck, A. B. Hayes, F. Wenander, M. Albers, B. Bastin, C. Bauer, A. Blazhev, S. Bönig, N. Bree, J. Cederkäll, T. Chupp, D. Cline, T. E. Cocolios, T. Davinson, H. D. Witte, J. Diriken, T. Grahn, A. Herzan *et al*., Nature (London) **497**, 199 (2013)
[35] P. A. Butler, L. P. Gaffney, P. Spagnoletti, K. Abrahams, M. Bowry, J. Cederkäll, G. de Angelis, H. De Witte, P. E. Garrett, A. Goldkuhle, C. Henrich, A. Illana, K. Johnston, D. T. Joss, J. M. Keatings, N. A. Kelly, M. Komorowska, J. Konki, T. Kröll, M. Lozano, B. S. Nara Singh, D. O'Donnell, J. Ojala, R. D. Page, L. G. Pedersen, C. Raison, P. Reiter, J. A. Rodriguez, D. Rosiak, S. Rothe, M. Scheck, M. Seidlitz, T. M. Shneidman, B. Siebeck, J. Sinclair, J. F. Smith, M. Stryjczyk, P. Van Duppen, S. Vinals, V. Virtanen, N. Warr, K. Wrzosek-Lipska, and M. Zielinska, Phys. Rev. Lett. **124**, 042503 (2020)
[36] P. A. Butler *et al*., Nat. Commun. **10**, 2473 (2019)
[37] M. M. R. Chishti, D. O'Donnell, G. Battaglia, M. Bowry, D. A. Jaroszynski, B. S. N. Singh, M. Scheck, P. Spagnoletti, and J. F. Smith, Nat. Phys. **16**, 853 (2020)
[38] A. Gyurkovich, A. Sobiczewski, B. Nerlo-Pomorska, and K. Pomorski, Phys. Lett. B **105**, 95 (1981)
[39] P. Möller, R. Bengtsson, B. G. Carlsson, P. Olivius, T. Ichikawa, H. Sagawa, and A. Iwamoto, At. Data Nucl. Data Tables **94**, 758 (2008)
[40] Y. S. Chen and Z. C. Gao, Phys. Rev. C **63**, 014314 (2000)
[41] Y.-J. Chen, Z.-C. Gao, Y.-S. Chen, and Y. Tu, Phys. Rev. C **91**, 014317 (2015)
[42] Z. P. Li, B. Y. Song, J. M. Yao, D. Vretenar, and J. Meng, Phys. Lett. B **726**, 866 (2013)
[43] S. Y. Xia, H. Tao, Y. Lu, Z. P. Li, T. Nikšić and D. Vretenar, Phys. Rev. C **96**, 054303 (2017)
[44] K. Nomura, L. Lotina, T. Nikšić, and D. Vretenar, Phys. Rev. C **103**, 054301 (2021)
[45] J. Engel and F. Iachello, Phys. Rev. Lett. **54**, 1126 (1985)
[46] D. Kusnezov and F. Iachello, Phys. Lett. B **209**, 420 (1988)
[47] K. Nomura, R. Rodríguez-Guzmán, and L. M. Robledo, Phys. Rev. C **92**, 014312 (2015)
[48] K. Nomura, R. Rodríguez-Guzmán, L. M. Robledo, J. E. García-Ramos, and N. C. Hernández, Phys. Rev. C **104**, 044324 (2021)
[49] K. Nomura, Phys. Rev. C **110**, 064306 (2024)
[50] J. M. Yao, E. F. Zhou, and Z. P. Li, Phys. Rev. C **92**, 041304(R) (2015)
[51] R. N. Bernard, L. M. Robledo, and T. R. Rodríguez, Phys. Rev. C **93**, 061302(R) (2016)
[52] E. F. Zhou, J. M. Yao, Z. P. Li, J. Meng, and P. Ring, Phys. Lett. B **753**, 227 (2016)
[53] P. Marević, J.-P. Ebran, E. Khan, T. Nikšić, and D. Vretenar, Phys. Rev. C **97**, 024334 (2018)
[54] R. Rodríguez-Guzmán, Y. M. Humadi, and L. M. Robledo, J. Phys. G: Nucl. Part. Phys. **48**, 015103 (2021)
[55] P. Bonche, P.-H. Heenen, H. Flocard, and D. Vautherin, Phys. Lett. B **175**, 387 (1986)
[56] P.-H. Heenen, J. Skalski, P. Bonche, and H. Flocard, Phys. Rev. C **50**, 802 (1994)
[57] L. M. Robledo and R. Rodríguez-Guzmán, J. Phys. G: Nucl. Part. Phys. **39**, 105103 (2012)
[58] M. Chen, T. Li, J. Dobaczewski, and W. Nazarewicz, Phys. Rev. C **103**, 034303 (2021)
[59] R. Rodríguez-Guzmán and L. M. Robledo, Phys. Rev. C **108**, 024301 (2023)
[60] B. Minh Loc, N. Le Anh, P. Papakonstantinou, and N. Auerbach, Phys. Rev. C **108**, 024303 (2023)
[61] P. Ring, Prog. Part. Nucl. Phys. **37**, 193 (1996)
[62] D. Vretenar, A. V. Afanasjev, G. A. Lalazissis, and P. Ring, Phys. Rep. **409**, 101 (2005)
[63] J. Meng, H. Toki, S. G. Zhou, S. Q. Zhang, W. H. Long, and L. S. Geng, Prog. Part. Nucl. Phys. **57**, 470 (2006)
[64] J. Meng, Relativistic Density Functional for Nuclear Structure (World Scientific, Singapore, 2016).
[65] S. Shen, H. Liang, W. H. Long, J. Meng, and P. Ring, Prog. Part. Nucl. Phys. **109**, 103713 (2019)
[66] K. Rutz, J. A. Maruhn, P. G. Reinhard, and W. Greiner, Nucl. Phys. A **590**, 680 (1995)
[67] S. E. Agbemava and A. V. Afanasjev, Phys. Rev. C **96**, 024301 (2017)
[68] K. Nomura, Phys. Rev. C **105**, 054318 (2022)
[69] J. Zhao and Z.-G. Wu, Phys. Rev. C **109**, 014303 (2024)
[70] J. C. Wang, Y. Tian, R. R. Xu, Y. Cui, X. Tao, X. D. Sun, Z. Zhang, Y. Zhang, Y. L. Han, Z. G. Ge, and N. C. Shu, Chin. Phys. C **48**, 064102 (2024)
[71] Y. Peng, J. Geng, and W. H. Long, Chin. Phys. C **49**, 074107 (2025)
[72] K. Nomura, D. Vretenar, T. Nikšić, and B.-N. Lu, Phys. Rev. C **89**, 024312 (2014)
[73] Z. P. Li, T. Nikšić, and D. Vretenar, J. Phys. G: Nucl. Part. Phys. **43**, 024005 (2016)
[74] W. Zhang and Y. F. Niu, Phys. Rev. C **96**, 054308 (2017)
[75] V. Prassa, Eur. Phys. J. A **58**, 183 (2022)
[76] L. S. Geng, J. Meng, and H. Toki, Chin. Phys. Lett. **24**, 1865 (2007)
[77] N. Wang and L. Guo, Sci. China Ser. G **52**, 1574 (2009)
[78] W. Zhang, Z. P. Li, S. Q. Zhang, and J. Meng, Phys. Rev. C **81**, 034302 (2010)
[79] W. Zhang, Z. P. Li, and S. Q. Zhang, Chin. Phys. C **34**, 1094 (2010)
[80] J. Y. Guo, P. Jiao, and X.-Z. Fang, Phys. Rev. C **82**, 047301 (2010)
[81] H. Huang and J. Y. Guo, Sci. Sin-Phys. Mech. Astron. **43**, 69 (2013)
[82] Y. T. Qiu, X. W. Wang, and J. Y. Guo, Phys. Rev. C **106**, 034301 (2022)
[83] Y. T. Qiu and J. Y. Guo, Nucl. Phys. A **1063**, 123181

(2025)
[84] P. Möller, A. J. Sierk, T. Ichikawa, and H. Sagawa, At. Data Nucl. Data Tables **109-110**, 1 (2016)
[85] T. Nikšić, D. Vretenar, and P. Ring, Phys. Rev. C **78**, 034318 (2008)
[86] G. A. Lalazissis, S. Karatzikos, R. Fossion, D. P. Arteaga, A. V. Afanasjev, and P. Ring, Phys. Lett. B **671**, 36 (2009)
[87] S. E. Agbemava, A. V. Afanasjev, and P. Ring, Phys. Rev. C **93**, 044304 (2016)
[88] Y. Cao, S. E. Agbemava, A. V. Afanasjev, W. Nazarewicz, and E. Olsen, Phys. Rev. C **102**, 024311 (2020)
[89] M. Kortelainen, T. Lesinski, J. Moré, W. Nazarewicz, J. Sarich, N. Schunck, M. V. Stoitsov, and S. Wild, Phys. Rev. C **82**, 024313 (2010)
[90] M. Kortelainen, J. McDonnell, W. Nazarewicz, P.-G. Reinhard, J. Sarich, N. Schunck, M. V. Stoitsov, and S. M. Wild, Phys. Rev. C **85**, 024304 (2012)
[91] M. Kortelainen, J. McDonnell, W. Nazarewicz, E. Olsen, P. G. Reinhard, J. Sarich, N. Schunck, S. M. Wild, D. Davesne, J. Erler, and A. Pastore, Phys. Rev. C **89**, 054314 (2014)
[92] E. Chabanat, P. Bonche, P. Haensel, J. Meyer, and R. Schaeffer, Phys. Scr. **1995**, 231 (1995)
[93] P. Klüpfel, P.-G. Reinhard, T. J. Bürvenich, and J. A. Maruhn, Phys. Rev. C **79**, 034310 (2009)
[94] G. A. Lalazissis, T. Nikšić, D. Vretenar, and P. Ring, Phys. Rev. C **71**, 024312 (2005)
[95] P. W. Zhao, Z. P. Li, J. M. Yao, and J. Meng, Phys. Rev. C **82**, 054319 (2010)
[96] Z. Xu and Z.-P. Li, Chin. Phys. C **41**, 124107 (2017)
[97] P. Jachimowicz, M. Kowal, and J. Skalski, At. Data Nucl. Data Tables **138**, 101393 (2021)
[98] R. Rodríguez-Guzmán and L. M. Robledo, Phys. Rev. C **103**, 044301 (2021)
[99] S. Goriely, S. Hilaire, M. Girod, and S. Péru, Phys. Rev. Lett. **102**, 242501 (2009)
[100] G. A. Lalazissis, J. König, and P. Ring, Phys. Rev. C **55**, 540 (1997)
[101] P. Holzer, U. Mosel, and W. Greiner, Nucl. Phys. A **138**, 241 (1969)
[102] J. Maruhn and W. Greiner, Z. Phys. **251**, 431 (1972)
[103] W. Greiner, J. Y. Park, and W. Scheid, Nuclear Molecules (World Scientific, Singapore, 1995).
[104] Z. Wang, W. Zhu, C. Zhong, and T. Fan, Nucl. Phys. A **989**, 81 (2019)
[105] J.-F. Berger, Ph.D. thesis, Université Paris-Sud, 1985.
[106] D. Regnier, N. Dubray, N. Schunck, and M. Verriere, Phys. Rev. C **93**, 054611 (2016)
[107] D. Regnier, N. Dubray, and N. Schunck, Phys. Rev. C **99**, 024611 (2019)
[108] Z. Li, S. Chen, M. Zhou, Y. Chen, and Z. Li, Phys. Rev. C **109**, 064310 (2024)
[109] Z. Li, Y. Su, L. Liu, Y. Chen, and Z. Li, Phys. Lett. B **866**, 139509 (2025)
[110] N. Dubray, J. P. Ebran, P. Carpentier, M. Frosini, A. Zdeb, N. Pillet, J. Newsome, M. Verrière, G. Accorto, and D. Regnier, arXiv: 2506.10745.
[111] A. S. Fernández, J. Dobaczewski, X. Sun, and H. Wibowo, arXiv: 2406.12545.
[112] L.-S. Geng, Ph.D. thesis, Peking University, 2007.
[113] W. Long, J. Meng, N. VanGiai, and S.-G. Zhou, Phys. Rev. C **69**, 034319 (2004)
[114] A. Bohr and B. R. Mottelson, Nuclear Structure, Vol. I (Benjamin, New York, 1969).
[115] V. I. Kuprikov and V. N. Tarasov, Phys. Atom. Nucl. **84**, 796 (2021)
[116] V. N. Tarasov, V. I. Kuprikov, V. V. Pilipenko, and D. V. Tarasov, Probl. Atom. Sci. Tech. **3**, 8 (2023)
[117] V. N. Tarasov, V. I. Kuprikov, and D. V. Tarasov, Probl. Atom. Sci. Tech. **5**, 16 (2024)
[118] K. Hagihara, T. Nakatsukasa, and N. Hinohara, Particles **8**, 72 (2025)
[119] A. Taninah, S. E. Agbemava, A. V. Afanasjev, and P. Ring, Phys. Lett. B **800**, 135065 (2020)
[120] Z. X. Liu, Y. H. Lam, N. Lu, and P. Ring, Phys. Lett. B **842**, 137946 (2023)
[121] E. Yüksel, T. Marketin, and N. Paar, Phys. Rev. C **99**, 034318 (2019)
[122] Y. Tian, Z. Y. Ma, and P. Ring, Phys. Lett. B **676**, 44 (2009)